Journal of Quantum Information Science, 2026, 16(1), 1-15
https://www.scirp.org/journal/jqis
ISSN Online: 2162-576X
ISSN Print: 2162-5751

Optomechanical Sensors Based on Exceptional Points

Foulla Dieudonné Platou[1], Djerandouba Ndjabaou Fabrice[2], Beuteubé Rianbé François[1], Koyambo-Konzapa Steve Jonathan[3]

[1]Department of Physics, Faculty of Exact and Applied Science, University of N'Djamena, N'Djamena, Chad
[2]Faculty of Science, Department of Physics, University of Ngaoundéré, Ngaoundéré, Cameroon
[3]Matter, Energy, and Radiation Laboratory (LAMER), University of Bangui, Bangui, Central African Republic
Email: foulladieudo@gmail.com, ndjabaufabriced@gmail.com, beuteubé2012@gmail.com, koyamboj@yahoo.fr Matter

How to cite this paper: Platou, F.D., Fabrice, D.N., François, B.R. and Jonathan, K.-K.S. (2026) Optomechanical Sensors Based on Exceptional Points. *Journal of Quantum Information Science*, **16**, 1-15.
https://doi.org/10.4236/jqis.2026.161001

Received: December 15, 2025
Accepted: January 19, 2026
Published: January 22, 2026

Abstract

We propose optomechanical sensors operating at exceptional points (EPs) by exploiting synthetic magnetism in a passive system. The system consists of two mechanically coupled resonators, optically excited through a phase-dependent phonon transfer mechanism. When a particular phase-matching condition of $\frac{\pi}{(2n+1)}$ is satisfied, a series of exceptional points emerges. Any perturbation breaks this condition, lifts the degeneracy, and induces a frequency splitting that varies with the square root of the perturbation intensity, leading to enhanced sensitivity. The introduction of quantum squeezing allows for the reduction of noise amplification effects and improves the sensitivity of EP-based sensors, indirectly also lowering the system's input optical power. By leveraging multiple EPs, this approach demonstrates enhanced sensitivity compared to anti-PT symmetric sensors under similar parameter conditions, paving the way for applications in mass detection, nanoparticle sensing, and environmental monitoring.

Keywords

Optomechanical, Exceptionnal Point, Synthetic Magnetism, Quantum Squeezing

1. Introduction

Optomechanics is the field of physics that studies the interaction between electromagnetic radiation and microscopic or nanoscopic mechanical objects. Since the advent of quantum mechanics, significant progress has been made in understand-

ing light-matter interactions, including phenomena such as quantum superposition, entanglement, and uncertainty relations [1] [2]. These advances have enabled the development of optomechanical systems with applications in precision detection [3] [4], metrology, and signal translation [5]. Optomechanical sensors [6] convert mechanical or optical signals into measurable outputs and are widely used in medicine, automotive technologies, environmental monitoring [7], and nanotechnology. In particular, these sensors have demonstrated strong potential for detecting extremely small masses, including viruses [8], nanoparticles [9], and pollutants, as well as for measuring temperature and salinity [10] [11]. Improving the sensitivity of these sensors remains a key challenge. A promising strategy for improving sensitivity is based on exploiting exceptional points.

Exceptional points [12]-[14] are singular degenerations of non-Hermitian systems where both eigenvalues and eigenvectors are simultaneously degenerate. Near an exceptional point, the system's response to external perturbations [15] [16] exhibits a square-root dependence, allowing for sensitivity improvements beyond that of conventional sensors. However, sensors based on exceptional points are often implemented in active systems requiring gain to compensate for losses, leading to time-parity symmetry [17]. Although gain facilitates the emergence of exceptional points, it also amplifies quantum noise and limits practical sensitivity. In this context, synthetic magnetism refers to an artificial gauge field for neutral bosonic excitations, such as phonons, which simulates the effect of a magnetic field via phase-dependent coupling. In the current system, synthetic phononic magnetism is implemented through a controlled phase in the mechanical coupling between two resonators, inducing a non-reciprocal phononic jump and allowing the emergence of exceptional points in a purely passive optomechanical system. The objective of this work is therefore to design a passive optomechanical sensor operating at exceptional points by combining synthetic magnetism and quantum compression [9] [18]-[21]. This approach allows for multiple exceptional points, improved sensitivity, and reduced operational power requirements. This work is organized as follows: Section II presents the theoretical model and derives the dynamic equations. Section III is devoted to analyzing the sensitivity improvement induced by synthetic magnetism and compression. Section IV concludes the work and discusses limitations and prospects.

2. Model and Dynamic Equations

The model considered here is an electromechanical circuit consisting of two coupled mechanical resonators excited by a common electric field source (**Figure 1**). We have also modeled its optomechanical equivalence. In what follows, we consider its optomechanical equivalence for the design of our optomechanical sensor at exceptional points under the requirement of synthetic magnetism. Radiation of frequency (ω_r) enters the frequency cavity (ω_c) through the optical part (fixed mirror in blue) and excites the two (2) mechanical resonators (moving mirrors) via an optical fiber. These two resonators will start moving under the action of the pressure force induced by the radiation (photons) in the cavity.

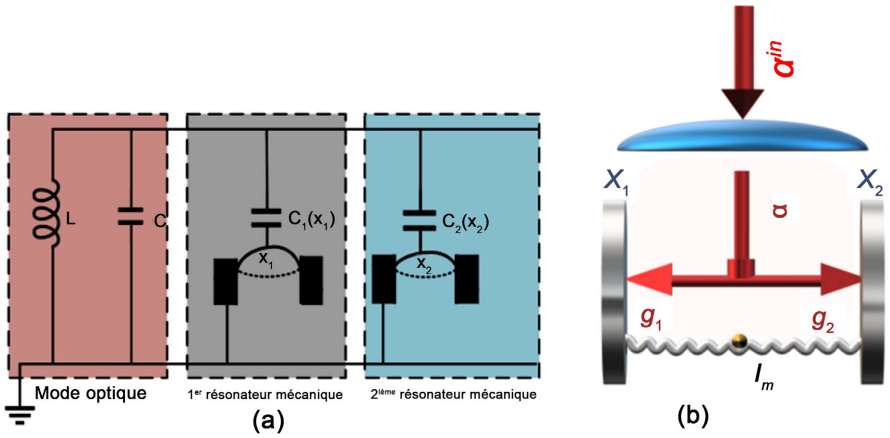

Figure 1. (a) Electromechanical system in which two mechanically coupled mechanical resonators are driven by a common electric field from an electric LC oscillator. (b) An optomechanical system equivalent to (a). J_m is the mechanical coupling dependent on the phase. θ.

The Hamiltonian ($\hbar = 1$) describing our system is

$$\mathrm{H_T} = \mathrm{H_{OM}} + \mathrm{H}_\gamma + \mathrm{H}_\kappa + \mathrm{H_{Drive}} + \mathrm{H_{Int}}$$

and with

$$\begin{cases} \mathrm{H_{OM}} = -\Delta a^\dagger a + \sum_{j=1,2}\left(\omega_j b_j^\dagger b_j - g_j a^\dagger a\left(b_j^\dagger + b_j\right) + \frac{1}{2}\epsilon_b\left(b_j^2 + b_j^{\dagger 2}\right)\right), \\ \mathrm{H_{Drive}} = i\sqrt{\kappa}\alpha^{in}\left(a + a^\dagger\right) \\ \mathrm{H_{Int}} = J_m\left(\mathrm{e}^{i\theta} b_1^\dagger b_2 + \mathrm{e}^{-i\theta} b_1 b_2^\dagger\right). \end{cases} \quad (1)$$

In this expression, $\mathrm{H_{OM}}$ represents the sum of the Hamiltonians of the optomechanical system with the optomechanical coupling force g. $a^\dagger\left(b_j^\dagger\right)$ and $a\left(b_j\right)$ $\left(j = 1,2\right)$ are the creation and annihilation operators of the cavity and mechanical resonators. The frequencies of the cavity and mechanical resonators are ω_{cav} and ω_j, respectively. $\mathrm{H_{Int}}$ and $\mathrm{H_{Drive}}$ are the interaction Hamiltonian of the two (2) mechanical resonators and the Hamiltonian of the incoming laser field, respectively. In particular, the quadratic part of the total Hamiltonian ($\mathrm{H_T}$) can be diagonalized with the compression transformation $\mathrm{S}_j\left(r_d\right) = \exp\left[r_d\left(b_j^2 - b_j^{\dagger 2}\right)\right]$ $\left(j = 1,2\right)$. This operator transforms by the Bogoliubov transformation [22] b à b_s as,

$$b_j^s = b_j \cosh\left(r_d\right) + b_j^\dagger \mathrm{e}^{-\phi_d} \sinh\left(r_d\right), \quad (2)$$

where the compression parameter r_d will be expressed later, and we set $\phi_d = 0$. Thus, we can simply write,

$$\begin{cases} b_j = b_j^s \cosh\left(r_d\right) - b_j^{s\dagger} \sinh\left(r_d\right) \\ b_j^\dagger = b_j^{s\dagger} \cosh\left(r_d\right) - b_j^s \sinh\left(r_d\right). \end{cases} \quad (3)$$

Using Eq. 03 in our Hamiltonian, we obtain the new Hamiltonian:

$$\begin{cases} \mathrm{H}_{\mathrm{OM}}^{S} = -\Delta a^{\dagger}a + \sum_{j=1,2}\Big(\big(\omega_j \cosh(2r_d) - \epsilon_b \sinh(2r_d)\big) b_j^{s\dagger} b_j^{s} \\ \qquad\qquad - \tilde{g}_j a^{\dagger} a\big(b_j^{s\dagger} + b_j^{s}\big) + \frac{1}{2}\big(\epsilon_b \cosh(2r_d) - \omega_j \sinh(2r_d)\big)\big(b_j^{s\dagger 2} + b_j^{s2}\big)\Big) \\ \mathrm{H}_{\gamma}^{\mathrm{S}} = -\sum_{j=1,2} \frac{i\gamma_j}{2} b_j^{s\dagger} b_j^{s} \\ \mathrm{H}_{\kappa}^{\mathrm{S}} = -\frac{i\kappa}{2} a^{\dagger} a \\ \mathrm{H}_{\mathrm{Drive}}^{\mathrm{S}} = i\sqrt{\kappa}\alpha^{in}\big(a + a^{\dagger}\big) \\ \mathrm{H}_{\mathrm{Int}}^{\mathrm{S}} = \tilde{J}_m\big(\mathrm{e}^{i\theta} b_1^{s\dagger} b_2^{s} + \mathrm{e}^{-i\theta} b_1^{s} b_2^{s\dagger}\big). \end{cases} \tag{4}$$

With $\mathrm{H}_{\kappa}^{\mathrm{S}}$ and $\mathrm{H}_{\gamma}^{\mathrm{S}}$ being the dissipation terms of the optical and mechanical parts, respectively. It is important to diagonalize our Hamiltonian in order to eliminate the quadratic terms. To do this, the following two conditions must be satisfied:

$$\begin{cases} \omega_j \cosh(2r_d) - \epsilon_b \sinh(2r_d) = \tilde{\omega}_j, \\ \epsilon_b \cosh(2r_d) - \omega_j \sinh(2r_d) = 0, \end{cases} \tag{5}$$

These conditions lead to the expressions,

$$\begin{cases} r_d = \frac{1}{4}\log\left(\frac{\omega_j + \epsilon_b}{\omega_j - \epsilon_b}\right) \\ \tilde{\omega}_j = \sqrt{\omega_j^2 - \epsilon_b^2}, \end{cases} \tag{6}$$

and the diagonalized Hamiltonian will take the form transformation:

$$\begin{cases} \mathrm{H}_{\mathrm{OM}}^{S} = -\Delta a^{\dagger}a + \sum_{j=1,2}\Big(\tilde{\omega}_j b_j^{s\dagger} b_j^{s} - \tilde{g}_j a^{\dagger} a\big(b_j^{s\dagger} + b_j^{s}\big)\Big) \\ \mathrm{H}_{\gamma}^{\mathrm{S}} = -\sum_{j=1,2} \frac{i\gamma_j}{2} b_j^{s\dagger} b_j^{s} \\ \mathrm{H}_{\kappa}^{\mathrm{S}} = -\frac{i\kappa}{2} a^{\dagger} a \\ \mathrm{H}_{\mathrm{Drive}}^{\mathrm{S}} = i\sqrt{\kappa}\alpha^{in}\big(a + a^{\dagger}\big) \\ \mathrm{H}_{\mathrm{Int}}^{\mathrm{S}} = \tilde{J}_m\big(\mathrm{e}^{i\theta} b_1^{s\dagger} b_2^{s} + \mathrm{e}^{-i\theta} b_1^{s} b_2^{s\dagger}\big), \end{cases} \tag{7}$$

with

$$\mathrm{H}_{\mathrm{T}}^{\mathrm{S}} = \mathrm{H}_{\mathrm{OM}}^{\mathrm{S}} + \mathrm{H}_{\gamma}^{\mathrm{S}} + \mathrm{H}_{\kappa}^{\mathrm{S}} + \mathrm{H}_{\mathrm{Drive}}^{\mathrm{S}} + \mathrm{H}_{\mathrm{Int}}^{\mathrm{S}}. \tag{8}$$

We can derive the dynamic equations of our system using Langevin's quantum equations [23].

$\dot{\mathcal{Q}} = \frac{\mathrm{d}\mathcal{Q}}{\mathrm{d}t} = i\left[\mathrm{H}_{\mathrm{T}}^{\mathrm{S}}, \mathcal{Q}\right] + \mathcal{N}$ with $\mathcal{Q} \equiv \left(a, b_j^{s}\right)$ and $\mathcal{N} \equiv \left(a^{in}, b_j^{s\,in}\right)$, with $\mathcal{N}$ the term noise.

Using the commutation relation with the different operators, we will have the following system of equations:

$$\begin{cases} \dot{a} = \left(i\left(\Delta + \sum_{j=1,2} \tilde{g}_j \left(b_j^{s\dagger} + b_j^s\right)\right) - \dfrac{\kappa}{2}\right) a + \sqrt{\kappa}\left(\alpha^{in} + a^{in}\right), \\ \dot{b}_1^s = -\left(\dfrac{1}{2}\gamma_1 + i\tilde{\omega}_1\right) b_1^s + i\tilde{g}_1 a^\dagger a - i\tilde{J}_m \mathrm{e}^{i\theta} b_2^s + \sqrt{\gamma_1} b_1^{s\,in}, \\ \dot{b}_2^s = -\left(\dfrac{1}{2}\gamma_2 + i\tilde{\omega}_2\right) b_2^s + i\tilde{g}_2 a^\dagger a - i\tilde{J}_m \mathrm{e}^{-i\theta} b_1^s + \sqrt{\gamma_2} b_2^{s\,in}. \end{cases} \tag{9}$$

The system of Equations (9) is a nonlinear system of equations, so it is convenient to linearize it. This linearization will allow us to simplify the analysis of the nonlinear system by approximating it with a linear model. By decomposing the field operators into $\mathcal{Q} = \langle \mathcal{Q} \rangle + \delta\mathcal{Q}$, where $\langle \mathcal{Q} \rangle$ is the coherent complex part of the operator and $\delta\mathcal{Q}$ is its associated fluctuation. Using the system of Equations (9) and replacing the bosonic operators a and b_j respectively by $a = \alpha + \delta a$ and $b_j^s = \beta_j + \delta b_j^s$ (wher $\alpha = \langle a \rangle$ and $\beta_j = \langle b_j^s \rangle$), We will have two parts after identification:

- Static part of average terms

$$\begin{cases} \dot{\alpha} = \left(i\tilde{\Delta} - \dfrac{\kappa}{2}\right)\alpha + \sqrt{\kappa}\alpha^{in}, \\ \dot{\beta}_1 = -\left(\dfrac{1}{2}\gamma_1 + i\tilde{\omega}_1\right)\beta_1 + i\tilde{g}_1 |\alpha|^2 - i\tilde{J}_m \mathrm{e}^{i\theta}\beta_2, \\ \dot{\beta}_2 = -\left(\dfrac{\gamma_2}{2} + i\tilde{\omega}_2\right)\beta_2 + i\tilde{g}_2 |\alpha|^2 - i\tilde{J}_m \mathrm{e}^{-i\theta}\beta_1. \end{cases} \tag{10}$$

- Part related to fluctuations

$$\begin{cases} \delta\dot{a} = \left(i\tilde{\Delta} - \dfrac{\kappa}{2}\right)\delta a + i\sum_{j=1,2} \tilde{g}_j \left(\delta b_j^{s\,\dagger} + \delta b_j^s\right)\alpha + \sqrt{\kappa} a^{in}, \\ \delta\dot{b}_1^s = -\left(\dfrac{1}{2}\gamma_1 + i\tilde{\omega}_1\right)\delta b_1^s + i\tilde{g}_1\left(\alpha^*\delta a + \delta a^\dagger \alpha\right) - i\tilde{J}_m \mathrm{e}^{i\theta}\delta b_2^s + \sqrt{\gamma_1} b_1^{s\,in}, \\ \delta\dot{b}_2^s = -\left(\dfrac{\tilde{\gamma}_2}{2} + i\tilde{\omega}_2\right)\delta b_2^s + i\tilde{g}_2\left(\alpha^*\delta a + \delta a^\dagger \alpha\right) - i\tilde{J}_m \mathrm{e}^{-i\theta}\delta b_1^s + \sqrt{\gamma_2} b_2^{s\,in}. \end{cases} \tag{11}$$

Effective hamiltonian of the systems

Under the condition of parameters $\kappa \gg \left(G, \gamma_j\right)$, we can adiabatically eliminate the cavity field in Equation (11) in order to obtain the effective mechanical system. To do this, we set,

$$\delta\tilde{a}_\kappa = \delta\tilde{a}\mathrm{e}^{\left(\frac{\kappa}{2}\right)t} \quad \text{et} \quad \delta\tilde{a} = \delta\tilde{a}_\kappa \mathrm{e}^{\left(-\frac{\kappa}{2}\right)t}, \tag{12}$$

We will assume that G_1 and G_2 are positive values and that $G_1 = G_2 = G$.

So, using the first equation of the system in Equation (11), we can derive the expression for $\delta\tilde{a}$ and then use it in the other two (2) equations of the system. Using the optical dissipation $\Gamma = \dfrac{4|G|^2}{\kappa}$, this leads us to:

$$\begin{cases} \delta\dot{\tilde{b}}_1^s = -\dfrac{1}{2}\gamma_1\delta\tilde{b}_1^s - \dfrac{\Gamma}{2}\left(\delta\tilde{b}_1^s + \delta\tilde{b}_2^s\right) + i\sqrt{\Gamma}\tilde{a}^{in} - i\tilde{J}_m\left(\mathrm{e}^{i\theta}\delta\tilde{b}_2^s\right) + \sqrt{\gamma_1}\tilde{b}_1^{s\,in}, \\ \delta\dot{\tilde{b}}_2^s = -\dfrac{\gamma_2}{2}\delta\tilde{b}_2^s - \dfrac{\Gamma}{2}\left(\delta\tilde{b}_1^s + \delta\tilde{b}_2^s\right) + i\sqrt{\Gamma}\tilde{a}^{in} - i\tilde{J}_m\left(\mathrm{e}^{-i\theta}\delta\tilde{b}_1^s\right) + \sqrt{\gamma_2}\tilde{b}_2^{s\,in}. \end{cases} \tag{13}$$

Using these transformations in Equation (1), we obtain

$$\begin{cases} \delta\dot{b}_1^s = -\left[i\tilde{\omega}_1 + \frac{1}{2}(\gamma_1 + \Gamma)\right]\delta b_1^s - \left(i\tilde{J}_m e^{i\theta} + \frac{\Gamma}{2}\right)\delta b_2^s + i\sqrt{\Gamma}\tilde{a}^{in\dagger} + \sqrt{\gamma_1}\tilde{b}_1^{s\,in}, \\ \delta\dot{b}_2^s = -\left[i\tilde{\omega}_2 + \frac{1}{2}(\gamma_2 + \Gamma)\right]\delta b_2^s - \left(i\tilde{J}_m e^{-i\theta} + \frac{\Gamma}{2}\right)\delta b_1^s + i\sqrt{\Gamma}\tilde{a}^{in\dagger} + \sqrt{\gamma_2}\tilde{b}_2^{s\,in}. \end{cases} \tag{14}$$

Then Equation (14) can be written in the following compact form,

$$\dot{\mathcal{X}} = -A\mathcal{X} - i\sqrt{\Gamma}a^{in\dagger}\mathbb{I}_2 + \mathcal{Y},$$

where we have by identification $\mathcal{X} = \begin{pmatrix} \delta b_1^s \\ \delta b_2^s \end{pmatrix}$ $\mathcal{Y} = \begin{pmatrix} \sqrt{\gamma_1} b_1^{s\,in} \\ \sqrt{\gamma_2} b_2^{s\,in} \end{pmatrix}$ $\mathbb{I}_2 = \begin{pmatrix} 1 \\ 1 \end{pmatrix}$ et

$$A = \begin{pmatrix} i\tilde{\omega}_1 + \frac{1}{2}(\gamma_1 + \Gamma) & i\tilde{J}_m e^{i\theta} + \frac{\Gamma}{2} \\ i\tilde{J}_m e^{-i\theta} + \frac{\Gamma}{2} & i\tilde{\omega}_2 + \frac{1}{2}(\gamma_2 + \Gamma) \end{pmatrix}, \tag{15}$$

We can write it in the form of the following Schrödinger equation by removing the noise terms,

$$i\frac{\partial \Psi}{\partial t} = \mathrm{H}_{\mathrm{eff}}\Psi, \tag{16}$$

where $\Psi = \begin{pmatrix} \delta b_1^s \\ \delta b_2^s \end{pmatrix}$ et

$$\mathrm{H}_{\mathrm{eff}} = \begin{pmatrix} \tilde{\omega}_1 - \frac{i}{2}(\gamma_1 + \Gamma) & \tilde{J}_m e^{i\theta} - \frac{i\Gamma}{2} \\ \tilde{J}_m e^{-i\theta} - \frac{i\Gamma}{2} & \tilde{\omega}_2 - \frac{i}{2}(\gamma_2 + \Gamma) \end{pmatrix}. \tag{17}$$

The eigenvalues of the system

We consider the matrix of Equation (17) to determine these associated eigenvalues.

$$\lambda_{\pm} = \frac{1}{2}(\tilde{\omega}_1 + \tilde{\omega}_2) - \frac{i}{4}\left(\gamma_{\mathrm{eff}}^1 + \gamma_{\mathrm{eff}}^2\right) \pm \frac{1}{4}\sigma. \tag{18}$$

where λ is the eigenvalue sought and with $\Delta\omega = \tilde{\omega}_1 - \tilde{\omega}_2$ et, $\Delta\gamma = \gamma_{\mathrm{eff}}^1 - \gamma_{\mathrm{eff}}^2$, $\sigma = \sqrt{\Upsilon - 16i\tilde{J}_m\Gamma\cos(\theta)}$, $\Upsilon = (2\Delta\omega - i\Delta\gamma)^2 + 16\tilde{J}_m^2 - 4\Gamma^2$, and $\gamma_{\mathrm{eff}}^j = \Gamma + \gamma_j$.

The sensitivity efficiency of our sensor depends on the lifting of degeneracy of the spectrum at the EP once our system is disturbed. The disturbance can be a nanoparticle or any mass deposit capable of disturbing the spectrum of our system. Therefore, we must locate the EP before examining the performance of the sensor. Assuming that

$$\gamma_1 = \gamma_2$$

and that there is no direct coupling between the mechanical resonators ($J_m = 0$), for example, σ is reduced to,

$$\Upsilon = (2\Delta\omega)^2 - 4\Gamma^2 \text{ and } \sigma = 2\sqrt{\Delta\omega^2 - \Gamma^2}, \tag{19}$$

leading to an exceptional point at

$$\Gamma = \Delta\omega,$$

this results from a symmetric anti-PT character of our system originating from the dissipative coupling induced by the cavity. By activating the phononic coupling ($J_m \neq 0$), with $\theta = \frac{\pi}{2}(2n+1)\ (n \in \mathbb{N})$ and this EP is shifted to if $n = 0$

$$\Gamma = \sqrt{\Delta\omega^2 + 4\tilde{J}_m^2}. \tag{20}$$

But for $n \neq 0$, we set $\theta = \pi/(2 \pm \epsilon)$, where ϵ is a perturbation force. This perturbation force leads us to the phase shift $\delta\theta = \pm\epsilon\frac{\pi}{2}$. The phase shift acts here on the eigenvalues given in Equation (18) as follows, and we will assume that the perturbation $\delta\theta$ is small, so we will have,

$$\lambda_{\pm}^{\delta\theta} = \xi \pm \frac{1}{4}\sqrt{\sigma^2 + 16i\tilde{J}_m\Gamma\delta\theta\sin(\theta)}. \tag{21}$$

Avec $\xi = \frac{1}{2}(\tilde{\omega}_1 + \tilde{\omega}_2) - \frac{i}{4}(\gamma_{\text{eff}}^1 + \gamma_{\text{eff}}^2)$

An exceptional point occurs when the eigenvalues of a non-Hermitian system coincide, leading to non-orthogonal eigenmodes. These points are described by complex conjugate eigenvalues and linearly dependent associated eigenvectors. By observing l'Équation (18), si $\sigma = 0$

$$\lambda_{\pm}^{\text{EP}} = \frac{1}{2}(\tilde{\omega}_1 + \tilde{\omega}_2) - \frac{i}{4}(\gamma_{\text{eff}}^1 + \gamma_{\text{eff}}^2), \tag{22}$$

degeneration corresponding to the exceptional point is observed.

3. Sensitivity Improvement with Synthetic Magnetism and Compression Amplitude Adjustment

3.1. Outstanding Points

The parameters used are $\omega_1 = \omega_m$, $\omega_2 = (1 + 5\times10^{-4})\omega_m$, $\kappa = 7.3\times10^{-2}\omega_m$, $\Delta = -\omega_m$, $g = 1.077\times10^{-4}\omega_m$, $\gamma_1 = 1.077\times10^{-5}\omega_m$, $\gamma_2 = \gamma_1$, $J_m = 2\times10^{-4}\omega_m$, $\theta = \frac{\pi}{2}$, $\epsilon_b = 3050\omega_m$, and $\Delta_m = 4000\omega_m$. In the following **Figure 2**, we observe the exceptional points that appear at a low value of our laser power thanks to the value of r_d, our compression parameter. We have the exceptional point for a value of $\alpha^{in} \sim [88]$ for $r_d = 0.5$ in **Figure 2**. In an experimental situation, it is therefore beneficial to take the compression parameter into account in order to generate exceptional points with low laser powers.

Natural Modes Disturbed Depending on Laser Power

Figure 3 shows the separation of the system's natural frequencies after a disturbance, which is represented by the dotted curve in the figure. The disturbance can be caused by the deposition of a mass on the system, illustrated by the yellow mass in our theoretical model, which modifies the properties of the system and shifts

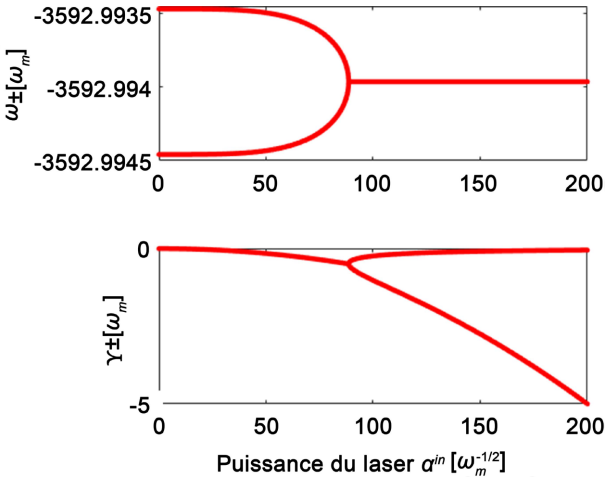

Figure 2. Exceptional points for $r_d = 0.5$.

the exceptional points. We can observe that the natural frequencies of the system separate after the disturbance, as indicated by the difference between the solid and dotted curves. This separation of natural frequencies is directly related to the disturbance and the sensitivity of the sensor. This is because the sensitivity of the sensor here is determined by the difference between the natural frequencies before and after the disturbance. The greater the separation of frequencies, the higher the sensitivity of the sensor, as shown in **Figure 3**. This means that the sensor is capable of detecting small disturbances with high accuracy for $r_d \neq 0$. In fact, the separation of natural frequencies is greatest at exceptional points, as shown in the figure when compression effects are considered. This indicates that exceptional points are points of maximum sensitivity for the sensor, which is a success compared to previous studies [24].

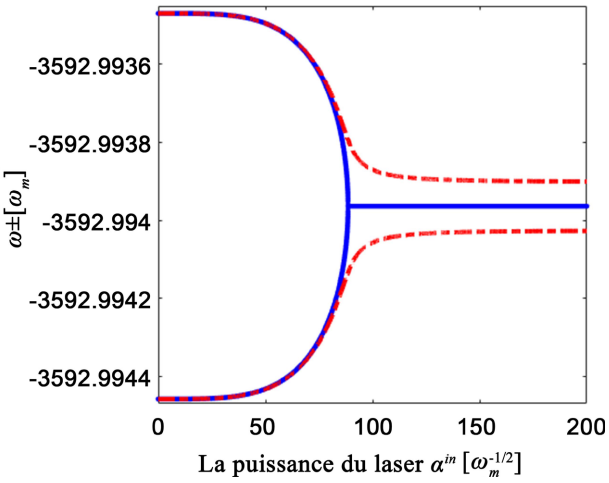

Figure 3. Exceptional points disturbed $r_d = 0.5$.

The eigenvalues of the effective Hamiltonian converge at exceptional points when specific phase and coupling conditions are satisfied. Any perturbation, such

as a mass deposit or phase deviation, lifts the degeneracy and induces a square root frequency separation (3).

3.2. Improving Sensitivity

We define the sensitivity of our sensor here as the absolute value of the frequency shift of a natural frequency relative to its reference. We thus define,

$$\Re\left(\Delta\lambda_{\pm}\right) \equiv \Re\left(\lambda_{\pm}^{\delta\theta} - \lambda_{\pm}\right)$$

Due to the high sensitivity at the EP level, the lifting of degeneracy associated with eigenvalues can be inferred as,

$$\Delta\lambda_{\pm} = \pm\frac{1}{4}\sqrt{\sigma^2 + 16i\tilde{J}_m\Gamma\delta\theta\sin\left(\theta\right)} \mp \frac{1}{4}\sigma. \tag{23}$$

This clearly shows the dependence of the square root on the perturbation $\delta\theta \neq 0$ as expected. Since sensitivity is defined as $\Re\left(\Delta\lambda_{\pm}^{\mathrm{EP}}\right)$, we can deduce that:

$$\Delta\lambda_{\pm}^{\mathrm{EP}} = \pm\frac{\left(1+i\right)}{2}\sqrt{2\delta\theta\tilde{J}_m\Gamma}. \tag{24}$$

This clearly shows the dependence of the square root on the perturbation $\delta\theta \neq 0$ as expected. Since sensitivity is defined as $\Re\left(\Delta\lambda_{\pm}^{\mathrm{EP}}\right)$, we can deduce that:

$$\Delta\omega_{\pm}^{\mathrm{EP}} = \Re\left(\Delta\lambda_{\pm}^{\mathrm{EP}}\right) = \pm\frac{\sqrt{2}}{2}\sqrt{\delta\theta\tilde{J}_m\Gamma}, \tag{25}$$

Therefore, for $\delta\theta = 0$, there is no division at the EP level.

The sensor sensitivity improvement factor is defined as,

$$\eta = \left|\frac{\Re\left(\Delta\lambda_{\pm}\right)}{\delta\theta}\right|. \tag{26}$$

This expression can be further simplified, leading to:

$$\eta = \left|\frac{\Delta\omega_{\pm}^{\mathrm{EP}}}{\delta\theta}\right| = \left|\frac{\pm\frac{1}{2}\sqrt{2\delta\theta\tilde{J}_m\Gamma}}{\delta\theta}\right| = \frac{\sqrt{\frac{\delta\theta\tilde{J}_m\Gamma}{2}}}{\left(\sqrt{\delta\theta}\right)^2} = \sqrt{\frac{\tilde{J}_m\Gamma}{2\delta\theta}}.$$

Figure 4 shows the sensitivity of the sensor as a function of the laser input power (α^{in}). As mentioned above, sensitivity is defined as the difference between the disturbed natural frequencies and the undisturbed natural frequencies. We can see in **Figure 4** that sensitivity is highest at the exceptional points for $r_d = 0.5$, where the separation of the eigenfrequencies is greatest. However, this result was predictable when we observe in the previous figure, a large separation of frequencies at the exceptional points. As shown by the solid black curve (for $r_d = 0$), we observe a low sensitivity of the sensor compared to the other two cases for values of $r_d \neq 0$. This means that the sensor is more sensitive to disturbances when we take into account the compression effects associated with the movements of mechanical objects in the cavity. These results highlight the importance of the compression effect we have considered here for improving the sensitivity of the sensor.

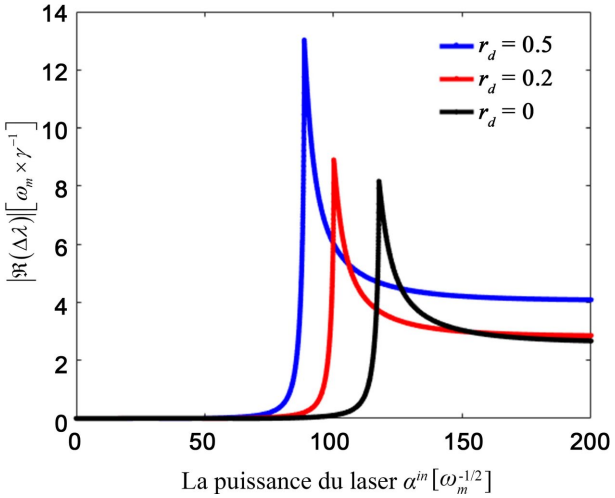

Figure 4. Sensitivity of the optomechanical sensor for different values of r_d and $\epsilon = 0.2$.

Figure 5 shows the sensitivity of the sensor as a function of phase θ for different values of compression amplitude (r_d). These results highlight the importance of exceptional points in improving sensor sensitivity and the possibility of detecting multiple disturbances. In addition, Figure 5 also shows the possibility of detecting multiple disturbances at different exceptional points. The solid red curve for $r_d = 0.5$ has a large amplitude, which is evident and means that the sensor can be used to detect multiple masses deposited on the system, opening up opportunities for multiple detection applications.

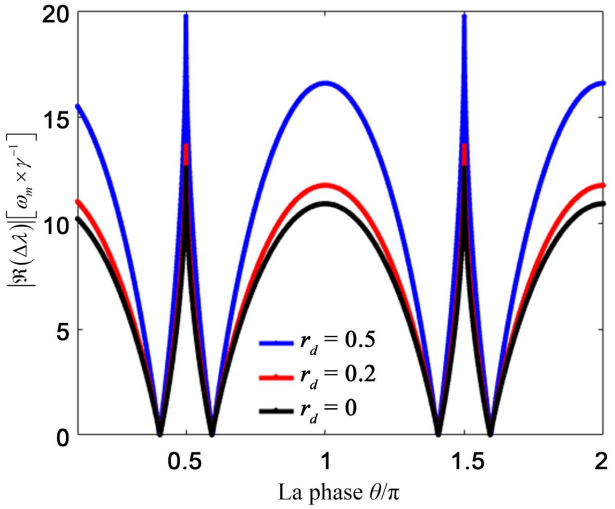

Figure 5. Sensitivity as a function of phase (θ) for three (3) different values of r_d and $\epsilon = 0.5$.

For comparison purposes, we choose two (2) other cases where we can also observe the sensitivity of the sensor. Figure 6 shows the sensitivity of the sensor when there is no direct coupling between the mechanical resonators. The system

still admits an exceptional point thanks to an anti-PT-symmetric characteristic induced by the dissipative coupling of the cavity. This curve shows lower sensitivity compared to the curves in Figure 6 for different values of the compression amplitude r_d, suggesting that combining the two types of perturbation can also improve the sensitivity of the sensor.

We can see in Figure 6 that when the compression amplitude value $r_d \neq 0$ (blue curve) is varied, there is considerable sensitivity compared to the red curve in this figure. However, the compression effect in the cavity also helps to improve the sensitivity of sensors using an anti-PT-symmetric characteristic induced by the dissipative coupling of the cavity.

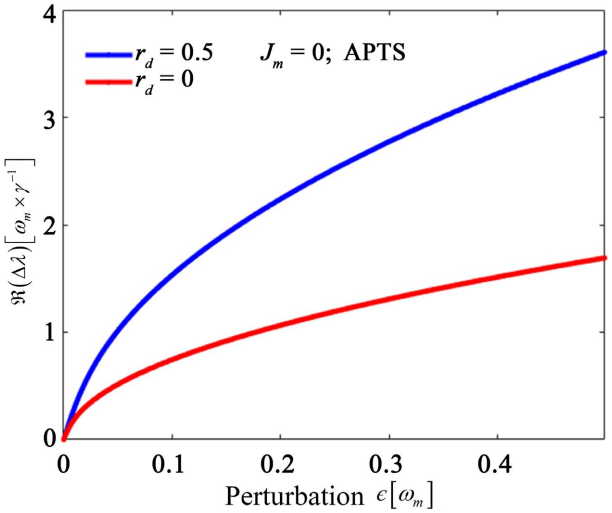

Figure 6. Sensitivity as a function of disturbance strength ϵ when there is no synthetic magnetism ($J_m = 0$) for two (2) values of r_d.

The curves in Figure 7 represent the sensitivity of the sensor when the disturbance is applied by modifying the quality factor of the mechanical resonators. This means that the disturbance mainly affects the damping ratio of the resonators, which also causes a shift in the natural frequencies. Compared to the previous figure, the curves in Figure 7 show slightly lower sensitivity, indicating that phase perturbation is more effective in improving sensor sensitivity. Indeed, when considering the effects of cavity compression, we observe a slightly better sensitivity (in blue) than that in red.

The Sensitivity Improvement Factor

Les courbes sur la Figure 8 for different values of r_d represent the factor of improvement in sensor sensitivity when there is no direct coupling between the mechanical resonators, the system still hosts an exceptional point thanks to an anti-PT-symmetric characteristic induced by the dissipative coupling of the cavity. However, the perturbation is applied by modifying both the phase and the quality factor of the resonators.

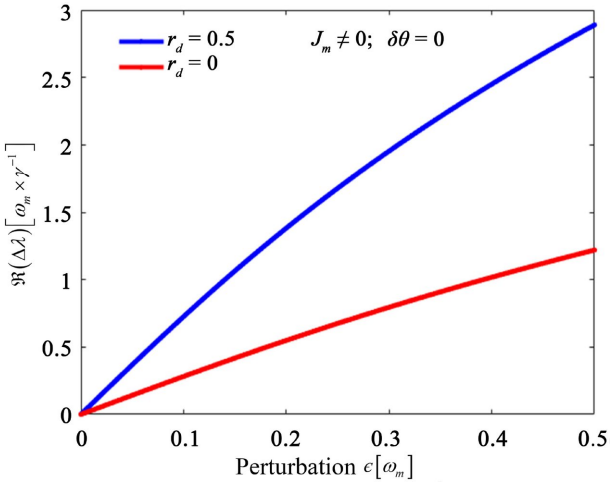

Figure 7. Sensitivity as a function of disturbance strength ϵ when $J_m \neq 0$ and $\delta\theta = 0$ for two (2) values of r_d.

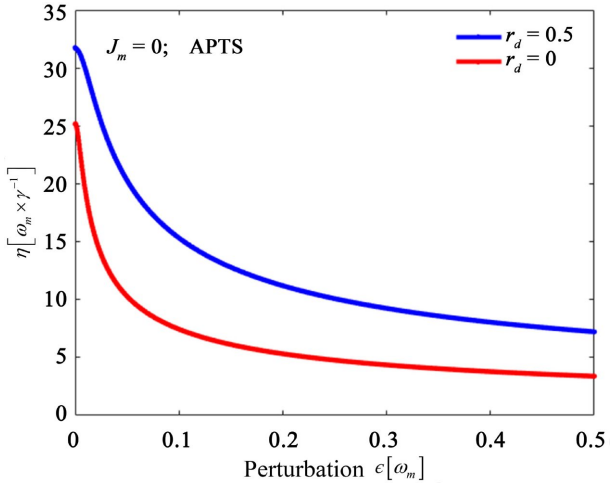

Figure 8. The sensitivity improvement factor as a function of the disturbance strength ϵ when synthetic magnetism ($J_m = 0$) for two (2) different values of r_d.

Compared to anti-PT-symmetric optomechanical sensors based solely on dissipative coupling, the present approach combines synthetic magnetism with quantum compression. Under normalized parameter conditions, this combination yields an enhanced sensitivity factor and larger frequency splitting while operating at lower input power. The following **Figure 9** shows the sensor sensitivity improvement factor when the disturbance is applied by modifying the quality factor of the mechanical reshonators. This figure shows that, although the disturbance of the quality factor can also improve the sensitivity of the sensor. This suggests that phase perturbation is more effective in improving sensor sensitivity. In this case, the blue curve has a greater amplitude than the red curve, which means that the effect of compression in the cavity allows the sensors to detect small mass particles.

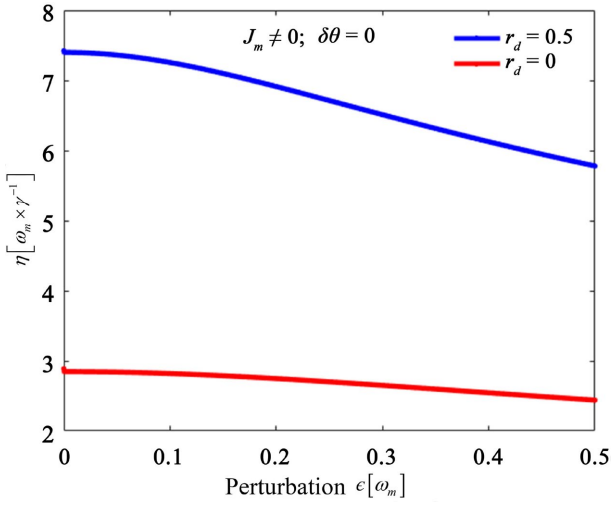

Figure 9. The sensitivity improvement factor as a function of the disturbance strength ϵ when $J_m \neq 0$ and $\delta\theta \neq 0$ for two (2) different values of r_d.

4. Conclusion

We have investigated a passive optomechanical sensor operating at exceptional points induced by synthetic magnetism and enhanced by quantum compression. The system supports multiple exceptional points without requiring gain, thereby significantly reducing the noise sources typically associated with sensors based on active exceptional points. The main contribution of quantum compression in this work lies in the elimination of noise amplification effects, allowing for a significant improvement in the sensitivity of the optomechanical sensor and the shift of exceptional points to experimentally accessible low-power regimes. Our approach shows that the combination of synthetic magnetism and quantum compression offers an effective route to improving optomechanical detection at exceptional points, with promising applications in precision measurement, mass detection, and environmental monitoring.

Conflicts of Interest

The authors declare no conflicts of interest regarding the publication of this paper.

References

[1] Zettili, N. (2003) Quantum Mechanics: Concepts and Applications. Wiley.

[2] Schütz, H. (2017) Quantum Optomechanics at Room Temperature. Ph.D Thesis, École Polytechnique Fédérale de Lausanne (EPFL).

[3] Ahmed, A.M., Mehaney, A. and Elsayed, H.A. (2021) Detection of Toluene Traces in Exhaled Breath by Using a 1D PC as a Biomarker for Lung Cancer Diagnosis. *The European Physical Journal Plus*, **136**, Article No. 626. https://doi.org/10.1140/epjp/s13360-021-01621-7

[4] Zaremanesh, M., Carpentier, L., Gharibi, H., Bahrami, A., Mehaney, A., Gueddida, A., *et al.* (2021) Temperature Biosensor Based on Triangular Lattice Phononic Crys-

tals. *APL Materials*, **9**, Article ID: 061114. https://doi.org/10.1063/5.0054155

[5] Bakker, E. and Telting-Diaz, M. (2002) Electrochemical Sensors. *Analytical Chemistry*, **74**, 2781-2800. https://doi.org/10.1021/ac0202278

[6] Liu, X., Liu, W., Ren, Z., Ma, Y., Dong, B., Zhou, G., *et al.* (2021) Progress of Optomechanical Micro/nano Sensors: A Review. *International Journal of Optomechatronics*, **15**, 120-159. https://doi.org/10.1080/15599612.2021.1986612

[7] El Jai, A. and Pritchard, A.J. (1987) Sensors and Actuators in Distributed Systems. *International Journal of Control*, **46**, 1139-1153. https://doi.org/10.1080/00207178708933956

[8] Francioso, P.A., Pennec, Y., Djafari-Rouhani, B., *et al.* (2010) Sensibilité optique et acoustique. Proc. 12èmes Journées de la Matière Condensée (JMC12).

[9] Woolley, M.J., Doherty, A.C., Milburn, G.J. and Schwab, K.C. (2008) Nanomechanical Squeezing with Detection via a Microwave Cavity. *Physical Review A*, **78**, Article ID: 062303. https://doi.org/10.1103/physreva.78.062303

[10] Qian, Y., Zhao, Y., Wu, Q.L. and Yang, Y. (2018) Review of Salinity Measurement Technology Based on Optical Fiber Sensors. *Sensors and Actuators B*: *Chemical*, **260**, 86-105. https://doi.org/10.1016/j.snb.2017.12.077

[11] Loubar, F. (2022). Quantum Kelvin: An Optomechanical Measure of Temperature by Quantum Correlations and Metrological Validation. Ph.D Thesis, HESAM Université.

[12] Heiss, W.D. (2012) The Physics of Exceptional Points. *Journal of Physics A*: *Mathematical and Theoretical*, **45**, Article ID: 444016. https://doi.org/10.1088/1751-8113/45/44/444016

[13] Miri, M. and Alù, A. (2019) Exceptional Points in Optics and Photonics. *Science*, **363**, eaar7709. https://doi.org/10.1126/science.aar7709

[14] Kazemi, H., Nada, M.Y., Mealy, T., Abdelshafy, A.F. & Capolino, F. (2019) Exceptional Points of Degeneracy Induced by Linear Time-Periodic Variation. *Physical Review Applied*, **11**, 014007. https://doi.org/10.1103/PhysRevApplied.11.014007

[15] Djorwé, P., Pennec, Y. and Djafari-Rouhani, B. (2019), Exceptional Point Enhances Sensitivity of Optomechanical Mass Sensors. *Physical Review Applied*, **12**. https://doi.org/10.1103/PhysRevApplied.12.024002

[16] Galland, N. (2019) Vers des systèmes opto-mécaniques et mesures de haute precision. Ph.D Thesis, Université Grenoble Alpes.

[17] Bender, C.M. and Boettcher, S. (1998) Real Spectra in Non-Hermitian Hamiltonians Having PT Symmetry. *Physical Review Letters*, **80**, 5243-5246. https://doi.org/10.1103/PhysRevLett.80.5243

[18] Feng, L., You, Y., Dong, H., Wang, F. and Gong, S. (2021) Enhancing Cross-Kerr Coupling via Mechanical Parametric Amplification. *Optics Express*, **29**, Article ID: 28835. https://doi.org/10.1364/oe.434677

[19] Tang, L., Tang, J., Chen, M., Nori, F., Xiao, M. and Xia, K. (2022) Quantum Squeezing Induced Optical Nonreciprocity. *Physical Review Letters*, **128**, Article ID: 083604. https://doi.org/10.1103/physrevlett.128.083604

[20] Timurdogan, E., Poulton, C.V., Byrd, M.J. and Watts, M.R. (2017) Electric Field-Induced Second-Order Nonlinear Optical Effects in Silicon Waveguides. *Nature Photonics*, **11**, 200-206. https://doi.org/10.1038/nphoton.2017.14

[21] Aggarwal, N., Cullen, T.J., Cripe, J., Cole, G.D., Lanza, R., Libson, A., *et al.* (2020)

Room-temperature Optomechanical Squeezing. *Nature Physics*, **16**, 784-788. https://doi.org/10.1038/s41567-020-0877-x

[22] Lesourd, J. (1947) Routes et trafic automobile en France. *L'information géographique*, **11**, 23-27. https://doi.org/10.3406/ingeo.1947.5229

[23] LAX, M. (1966) Classical Noise IV: Langevin Methods. *Reviews of Modern Physics*, **38**, 541-566. https://doi.org/10.1103/revmodphys.38.541

[24] Tchounda, S.R.M., Djorwé, P., Engo, S.G.N. and Djafari-Rouhani, B. (2023) Sensor Sensitivity Based on Exceptional Points Engineered via Synthetic Magnetism. *Physical Review Applied*, **19**, Article ID: 064016. https://doi.org/10.1103/physrevapplied.19.064016